© 2019. Published by The Company of Biologists Ltd | Development (2019) 146, dev164293. doi:10.1242/dev.164293

RESEARCH ARTICLE

The *C. elegans* heterochronic gene *lin-28* coordinates the timing of hypodermal and somatic gonadal programs for hermaphrodite reproductive system morphogenesis

Sungwook Choi and Victor Ambros*

ABSTRACT

C. elegans heterochronic genes determine the timing of expression of specific cell fates in particular stages of developing larvae. However, their broader roles in coordinating developmental events across diverse tissues have been less well investigated. Here, we show that loss of *lin-28*, a central heterochronic regulator of hypodermal development, causes reduced fertility associated with abnormal somatic gonadal morphology. In particular, the abnormal spermatheca-uterine valve morphology of *lin-28(lf)* hermaphrodites traps embryos in the spermatheca, which disrupts ovulation and causes embryonic lethality. The same genes that act downstream of *lin-28* in the regulation of hypodermal developmental timing also act downstream of *lin-28* in somatic gonadal morphogenesis and fertility. Importantly, we find that hypodermal expression, but not somatic gonadal expression, of *lin-28* is sufficient for restoring normal somatic gonadal morphology in *lin-28(lf)* mutants. We propose that the abnormal somatic gonadal morphogenesis of *lin-28(lf)* hermaphrodites results from temporal discoordination between the accelerated hypodermal development and normally timed somatic gonadal development. Thus, our findings exemplify how a cell-intrinsic developmental timing program can also control proper development of other interacting tissues, presumably by cell non-autonomous signal(s).

This article has an associated 'The people behind the papers' interview.

KEY WORDS: Heterochronic pathway, Lin-28, Morphogenesis, Reproductive system, Somatic gonad

INTRODUCTION

Heterochrony refers to modes of developmental alterations of an organism in which genetic changes lead to either accelerated or delayed development of certain body parts relative to others, in the context of evolution (Keyte and Smith, 2011; Klingenberg, 1998) or in experimental organisms (Ambros and Horvitz, 1984, 1987). Genetic mutations causing heterochrony in the nematode *Caenorhabditis elegans* identified a gene regulatory network, the 'heterochronic pathway', that governs the relative timing of developmental events during the four larval stages (L1-L4). Loss-of-function *(lf)* mutations of *lin-14* or *lin-28* result in precocious development via the skipping of hypodermal cell fates specific to one or more larval stages (Ambros and Horvitz, 1984, 1987). In contrast, *lin-4(lf)* and *let-7(lf)* mutations prevent the normal progression of certain stage-specific cell fates, leading to abnormal repetition of larval stages (Ambros and Horvitz, 1984; Reinhart et al., 2000).

lin-28 encodes a conserved RNA-binding protein containing one cold shock domain and two zinc-finger domains. The mammalian homolog of LIN-28 is implicated in diverse biological processes, including tumorigenesis, pluripotency and metabolism (Piskounova et al., 2011; Yu et al., 2007; Zhang et al., 2016; Zhu et al., 2011). In *C. elegans*, expression of LIN-28 is highest in the late embryo and L1 stages, and decreases from the L2 stage onwards. LIN-28 is primarily expressed in the hypodermis, neurons and muscle. *lin-28(lf)* mutants skip L2-specific hypodermal cell fates, resulting in precocious expression of L3, L4 and adult hypodermal fates (Moss et al., 1997; Seggerson et al., 2002). Thus, in the wild type, *lin-28* functions in early larval stages to specify the proper timing of the L2-to-L3 cell fate transitions. *lin-28* does this by promoting expression of the HBL-1 transcription factor, and by preventing premature expression of mature *let-7* microRNA (Abbott et al., 2005; Vadla et al., 2012; Van Wynsberghe et al., 2011).

Here, we have investigated the role of *lin-28* in maintaining the fertility of *C. elegans* hermaphrodites. The hermaphrodite gonad consists of germ cells, which originate from proliferation of two germline precursor cells (Z2 and Z3), and somatic gonadal tissues, which are derived from two somatic precursor cells (Z1 and Z4) located within the gonadal primordium of L1 larvae (Kimble and Hirsh, 1979). Somatic gonadal development occurs during the L1-L4 larval stages and is characterized by stage-specific patterns of cell division, morphogenesis and differentiation into tissues with specific functions, including the gonadal sheath cells, spermatheca, spermathecal-uterine valve (Sp-Ut valve), uterus and uterine seam (utse) cells. During ovulation, mature oocytes are released to the spermatheca for fertilization. Post-fertilization, the embryo exits from the spermatheca into the uterus. Efficient ovulation, fertilization and spermathecal exit are crucial for optimal reproductive capacity of *C. elegans* hermaphrodites, and mutants defective in these processes exhibit reduced fertility (Iwasaki et al., 1996; Kariya et al., 2004; Kovacevic and Cram, 2010).

Our results show that certain aspects of somatic gonadal development are abnormal in *lin-28(lf)* hermaphrodites, reflected by abnormal morphology of the uterus, uterine seam and Sp-Ut valve. These morphological defects, particularly the abnormal Sp-Ut valve, dramatically limit *lin-28(lf)* fertility. Our results further indicate that the normal development of the somatic gonad relies on temporal coordination of hypodermal developmental events with somatic gonadal events, and that *lin-28* acts in the hypodermis to specify a schedule of hypodermal events that is properly coordinated with a corresponding schedule of somatic gonadal developmental events. We demonstrate that the hypodermal function of *lin-28* is sufficient to regulate somatic

Program in Molecular Medicine, University of Massachusetts Medical School, Worcester, MA 01605, USA.

*Author for correspondence (victor.ambros@umassmed.edu)

S.C., 0000-0003-0328-2421; V.A., 0000-0002-5562-5345

Received 14 February 2018; Accepted 4 February 2019

Development (2019) 146, dev164293. doi:10.1242/dev.164293

gonadal development non-autonomously, consistent with a role for *lin-28* and downstream heterochronic genes, in controlling the hypodermal components of crucial developmental signaling between the gonad and hypodermis.

RESULTS

lin-28(lf) mutants exhibit defects in embryo production and embryonic viability

lin-28(n719) hermaphrodites produce fewer larval progeny than wild-type hermaphrodites (Fig. 1A). *lin-28(n719)* mutants are unable to lay eggs, owing to precocious vulva development, which results in abnormal vulva morphogenesis (Euling and Ambros, 1996). Like other egg-laying defective mutants, *lin-28(lf)* hermaphrodites contain their entire brood of embryos trapped inside the limited space of the somatic gonad. To test whether the reduced number of progeny of *lin-28(lf)* hermaphrodites could be simply the result of their egg-laying defect, we compared the number of progeny of *lin-28(n719)* hermaphrodites with that of *lin-2(e1309)*. *lin-2(e1309)* mutants exhibit defects in egg laying due to their vulvaless phenotype, which results from cell lineage defects not related to developmental timing (Hoskins et al., 1996). *lin-28(n719)* mutants produce substantially fewer progeny than *lin-2(e1309)* (Fig. 1A), suggesting the reduced brood of *lin-28(n719)* animals is not merely the result of an egg-laying defect. To quantify embryo production in *lin-28(n719)* hermaphrodites, we dissected mature gravid hermaphrodites and counted the embryos retained inside. *lin-28(n719)* gravid adults contained fewer embryos than *lin-2(e1039)* animals (Fig. 1B), indicating that *lin-28(n719)* mutants are defective in embryo production. To test embryonic viability, we harvested embryos from dissected gravid adults, and counted the number that hatched and developed into larvae. Approximately 70% of *lin-28(n719)* embryos failed to develop, whereas essentially all of the *lin-2(e1309)* embryos were viable (Fig. 1C). These results suggest that reduced embryo production and embryonic lethality contribute to the reduced progeny number of *lin-28(n719)* mutants. *lin-28(n719)* mutants also displayed these same defects at 20°C, although at a somewhat reduced penetrance compared with 25°C (Fig. S1). We conducted all our subsequent experiments at 25°C, where those defects are most prominent.

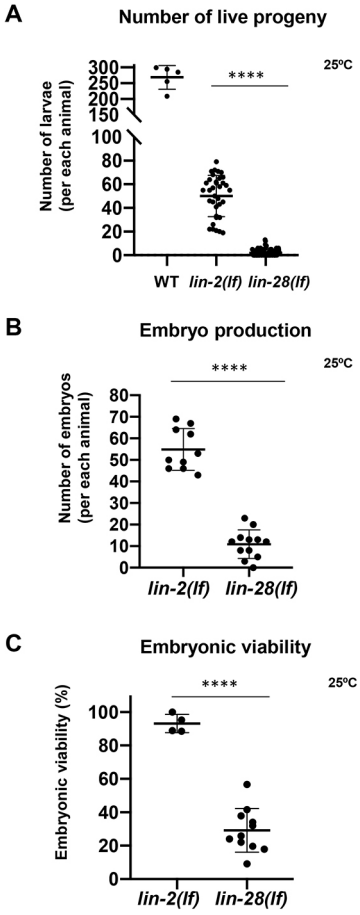

Fig. 1. *lin-28(lf)* hermaphrodites have reduced brood size and exhibit defects both in embryo production and embryonic viability. (A) Number of live progeny per hermaphrodite for wild type (strain N2), *lin-2(e1309)* and *lin-28(n719)* mutants at 25°C. *lin-2(e1309)* mutants are used as egg-laying defective controls; both *lin-2(e1309)* and *lin-28(n719)* hermaphrodites are unable to lay eggs. (B) Number of embryos per hermaphrodite for *lin-28(n719)* and *lin-2(e1309)* mutants at 25°C (dissected from gravid adults 60 h after initiation of synchronized larval development by feeding starved L1s). (C) Viability of mutant embryos dissected from *lin-28(n719)* and *lin-2(e1309)* hermaphrodites at 25°C. % viability=100×(viable hatched larvae/total embryos). Number of animals≥15 per assay; number of independent replicate assays=11 for *lin-28(n719)*, 4 for *lin-2(e1309)*. Data are mean±s.d. analyzed using an unpaired *t*-test, ****P<0.0001.

We also performed tissue-specific RNAi experiments using *rrf-1(lf)* and *ppw-1(lf)*, and observed that somatic knockdown of *lin-28* caused greater reduction of total number of progeny than did germline knockdown of *lin-28* (Fig. S2). This suggests the fertility defects of *lin-28(lf)* mutants are mainly due to somatic absence of *lin-28*.

Defects in ovulation and spermathecal exit cause reduced embryo production in *lin-28(lf)* mutants

To investigate the cause of reduced embryo production in *lin-28(n719)* mutants, we checked whether ovulation and spermathecal exit proceed normally. We examined the spermatheca of *lin-28(n719)* mutants using the expression of a spermatheca reporter, *fkh-6p::GFP* (Chang et al., 2004). Approximately 70% of *lin-28(n719)* adults contained embryos in their spermathecae, whereas fewer than 10% of wild-type spermathecae contained embryos (Fig. 2A,B). Unlike in the wild type, many embryos in *lin-28(n719)* hermaphrodites had undergone multiple rounds of cell division inside the spermathecae. This suggests that *lin-28(n719)* mutants have defects in the process of spermathecal exit. We used time-lapse video microscopy to monitor the first ovulation and spermathecal exit (Movies 1, 2). In wild-type hermaphrodites, ovulation, fertilization and spermathecal exit of an individual embryo happens within 20 min (McCarter et al., 1999). By contrast, we observed that for ∼50% of *lin-28(n719)* hermaphrodites, the first ovulated embryo remained in the spermatheca for more than 60 min (Fig. 2E; Movie 2).

Next, we addressed whether ovulation is also defective in *lin-28(n719)* mutants. The presence of endomitotically replicating (Emo) oocytes is a characteristic of ovulation mutants (Iwasaki et al., 1996), where oocytes undergo several rounds of DNA replication without ovulation and fertilization. Gonadal DAPI staining revealed that some *lin-28(n719)* hermaphrodites contain endomitotic oocytes (Fig. 2D) in the oviduct. We speculate that the defective ovulation in *lin-28(n719)* mutants may result from impairment of the spermathecal exit process, wherein the presence of fertilized embryos trapped within the limited spermathecal space would prevent subsequent entry of mature oocytes. We conclude that the poor fertility of *lin-28(n719)* mutants is the consequence of embryos becoming trapped in the spermathecae, stalling subsequent ovulation.

Development (2019) 146, dev164293. doi:10.1242/dev.164293

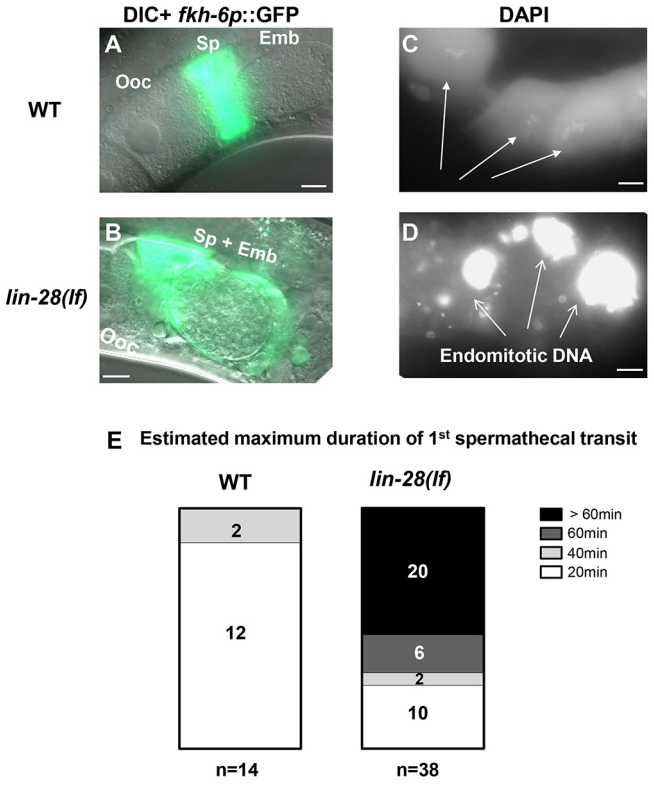

Fig. 2. *lin-28(lf)* hermaphrodites have defects in exit of embryos from the spermatheca, and defects in ovulation. (A,B) Spermatheca labeled by *fkh-6p::GFP* of representative wild-type and *lin-28(n719)* adult hermaphrodites. (A) In the wild type, oocytes (Ooc) pass into the spermatheca (Sp), where they are fertilized, and rapidly exit as a one-cell embryo (Emb). Therefore, most spermathecae are not observed to contain an embryo. (B) In a *lin-28(n719)* hermaphrodite, an embryo (around ~150 cells) was trapped in the spermatheca. (C,D) DAPI staining of oocytes in wild-type (C) and *lin-28(n719)* hermaphrodites. (C) In the wild type, individual oocytes (Ooc) contained a haploid complement of condensed chromosomes (arrows). (D) In the *lin-28(n719)* mutant, endomitotic DNA was evidenced by an excessively bright DAPI signal in the oviduct before spermathecae, a characteristic of ovulation-defective mutants. Scale bars: 10 µm. (E) Distribution of estimated maximum duration of 1st spermathecal transit to uterus in wild type and *lin-28(lf)* mutants (see Materials and Methods).

Sp-Ut valve morphogenesis, uterine lumen formation and utse cell migration are abnormal in *lin-28(lf)* mutants

Spermathecae in *C. elegans* hermaphrodites consist of two rows of 12 cells forming a long tube structure at the young adult stage (Gissendanner et al., 2008; Kimble and Hirsh, 1979). Long spermathecal tube structures, labeled using *fkh-6p::GFP*, are observed in the *lin-28(n719)* mutants at the 4th stage (Fig. 3B), which corresponds to L4 and adult stage in wild type (see Fig. 6C). Wild-type spermathecae become constricted horizontally as somatic gonadal tissues continue morphogenesis before the first ovulation. *lin-28(n719)* spermathecae exhibited a similar constricted and extended morphology as in the wild type (Fig. 3A,B). Overall, we did not detect appreciable differences in spermathecal morphology between wild-type animals and *lin-28(n719)* mutants.

The Sp-Ut valve connects the spermatheca to the uterus in wild-type hermaphrodites, and serves as a portal through which fertilized embryos exit the spermatheca into the uterus (McCarter et al., 1999). The mature Sp-Ut valve consists of the toroidal syncytium and the core cell syncytium. We characterized Sp-Ut valve structure in *lin-28(n719)* mutants using a *cog-1::GFP* reporter, which is expressed in the Sp-Ut valve core cell syncytium from the late L3 or early L4 stage (Palmer et al., 2002). In wild-type animals, the core cell syncytium stretches during the L4 stage, and in young adults, the Sp-Ut valve core forms a dumbbell-like structure with one end in the spermatheca and the other end in the uterus (Fig. 3C). Although we observed apparently normal expression of *cog-1::GFP* in the Sp-Ut valve region of *lin-28(n719)* mutants in late 3rd larval stage, the core cell stretching did not occur and the Sp-Ut valve core remained as a single lobe structure in 4th stage animals (Fig. 3D). This observation indicates that Sp-Ut valve morphology is abnormal in *lin-28(n719)* mutants, suggesting the connection between the spermatheca and the uterus is also disrupted. We conclude that the aberrant connection between the uterus and the spermatheca associated with the abnormal morphology of the Sp-Ut valve causes the spermathecal exit defect in *lin-28(lf)* mutants. To assess whether the abnormal Sp-Ut valve morphology of *lin-28(n719)* could reflect somatic gonadal cell lineage defects analogous to the precocious hypodermal cell lineages exhibited by *lin-28(n719)* (Ambros and Horvitz, 1984), we investigated whether the Sp-Ut valve syncytium in the mutant contains a normal number of nuclei as in the wild type. The Sp-Ut valve is derived from daughter cells of the dorsal uterine lineage, and the valve core syncytium comprises a fusion of two cells (Kimble and Hirsh, 1979). We used confocal microscopy to count the number of nuclei in the Sp-Ut valve core region based on labeling by *cog-1::GFP*. Two nuclei were present in the Sp-Ut valve core cell of both wild-type and *lin-28(n719)* mutants, suggesting the morphological defect is not caused by abnormal cell division in the lineage generating the Sp-Ut valve core (Fig. S3A,B).

In addition to the abnormal Sp-Ut valve morphology, other somatic gonadal defects were evident in *lin-28(n719)* mutants. In wild-type animals, the uterine lumen forms between the dorsal and ventral uterus during the L4 stage, when uterine toroidal cells fuse to generate a syncytium (Newman et al., 1996). In *lin-28(n719)* mutants at the 4th stage, we observed abnormally small, incompletely connected and/or less elongated uterine luminal structures, compared with the wild type (Fig. S4B,C).

The uterine seam (utse) is a component of the hermaphrodite somatic gonad that mediates structural attachment between the hypodermis and uterus (Newman and Sternberg, 1996). The utse syncytium forms in the early L4 stage and extends laterally during progression to mid L4. The utse connects the uterus to the seam cells laterally and also to uv1 and the vulva. *egl-13p::GFP* is expressed in the nuclei of π cell lineage, the products of which include the utse cells, from late L3 to L4 stages (Ghosh and Sternberg, 2014). Utse cells labeled by *egl-13p::GFP* migrated laterally in wild-type hermaphrodites (Fig. S5A,B). However, the utse nuclei did not migrate during the 4th stage in *lin-28(n719)* mutants, although *egl-13p::GFP(+)* cells were detected in the utse region (Fig. S5C,D).

lin-28(n719);lin-2(e1309) double mutants, which lack vulva formation, have the same somatic gonadal defects as *lin-28(n719)* mutants, implying these defects are not indirect consequences of the abnormal vulval morphology in *lin-28(n719)* mutants (Fig. S6). The defects in uterine lumen formation and utse cell migration in *lin-28(n719)* mutants, together with their Sp-Ut valve morphological defects, suggest that *lin-28* activity is required for multiple aspects of proper hermaphrodite somatic gonadal development.

Eggshell integrity is compromised in *lin-28(lf)* mutant embryos

To investigate the embryonic lethality in *lin-28(n719)* mutants, we dissected embryos from adult hermaphrodites and imaged the

Development (2019) 146, dev164293. doi:10.1242/dev.164293

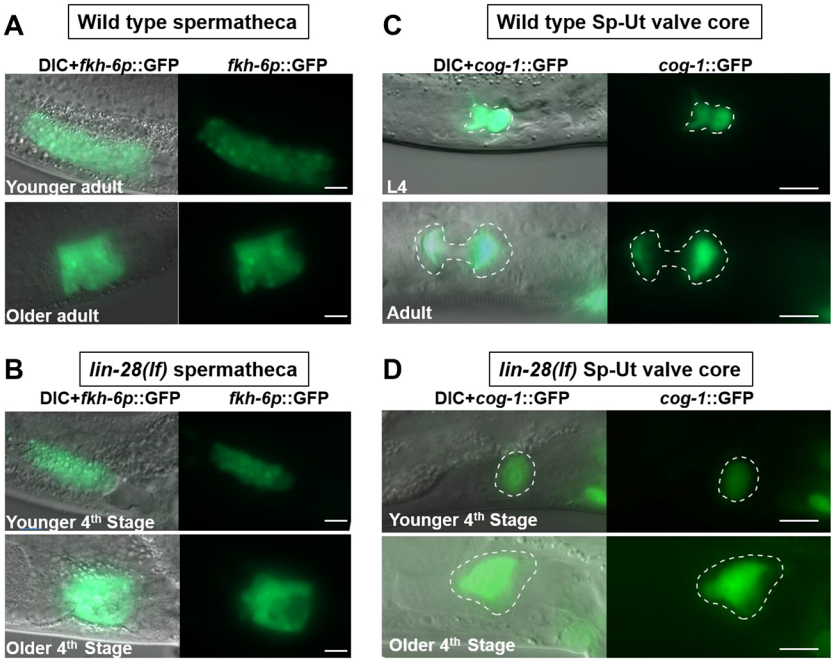

Fig. 3. *lin-28(lf)* mutants show essentially normal spermathecal primordium structure, but display defects in spermathecal-uterine (Sp-Ut) valve morphology. Spermathecal primordium visualized by *fkh-6p::GFP* expression (A,B) and Sp-Ut valve core structure visualized by *cog-1::GFP* expression (C,D) in wild type and *lin-28(n719)* hermaphrodites at successive times in the advancement towards the first ovulation. In each panel, the upper images are of hermaphrodites at the L4 or early young adult stage; the lower images are of hermaphrodites somewhat later in development, just before the time of first ovulation. [*lin-28(n719)* hermaphrodites skipped one larval stage; therefore, the '4th stage' corresponds to L4 and adult stage in wild type (see Fig. 6).] (A,B) In both wild type and *lin-28(n719)* mutants, similar tube-shaped spermathecal primordia were detected, which contracted horizontally to form similar sac-like structures in older adults (A,B, lower panels). (C,D) Sp-Ut valve core structure (outlined) labeled by *cog-1::GFP* at successive stages in L4-adult developmental progression of a wild type and *lin-28(n719)* hermaphrodite. (C) In wild type, the Sp-Ut valve core stretches to form a fully developed 'dumbbell' structure, with one lobe residing in the spermatheca and the other lobe in the uterus. The distance between each lobe shown here was ~10 µm. (D) In *lin-28(n719)* mutants, the Sp-Ut valve core does not stretch and remains as a 'single lobe' structure, indicating an abnormal connection between the spermatheca and uterus in the mutants. Scale bars: 10 µm.

isolated embryos. The *lin-28(n719)* embryos displayed abnormal irregular shapes (Fig. 4A), reminiscent of the misshapen phenotypes exhibited by egg-shell mutants (Johnston et al., 2006; Maruyama et al., 2007; Zhang et al., 2005). The *C. elegans* eggshell, formed rapidly after fertilization in the spermatheca, consists of chitin, lipid and structural proteins, and functions as a protective barrier around the embryo. Eggshell abnormalities often result in embryo lethality (Johnston et al., 2010).

Chitin-binding domain-protein 1 (CBD-1) is a component of the eggshell cortex, and *cbd-1::mcherry* expression marks the periphery of wild-type embryos (Allen et al., 2014; Johnston et al., 2010). *cbd-1::mcherry* expression was evident surrounding embryos from *lin-28(n719)* hermaphrodites, indicating that an eggshell does form (Fig. 4B). The wild-type eggshell is impermeable to the lipophilic dye FM4-64 (Johnston et al., 2006), but, in our study, about 50% of *lin-28(n719)* embryos were permeable to FM4-64, while around 10% of *lin-2(e1309)* embryos were permeable (Fig. 4C).

This finding indicates that eggshell integrity is compromised in embryos produced by *lin-28(n719)* mutants. In support of this conclusion, *lin-28(n719)* embryos also exhibited osmotic stress sensitivity. Embryos from wild-type hermaphrodites maintained their oval shape upon exposure to 0, 150 and 300 mM KCl, whereas embryos from *lin-28(n719)* animals swelled up in 0 or 150 mM KCl (Fig. 4D). Interestingly, embryos of *fln-1(tm545)* mutants, which have defective spermathecal exit (Kovacevic and Cram, 2010), also exhibited permeability to FM4-64 (Fig. 4C), suggesting that abnormally prolonged residence in the spermatheca may result in compromised eggshell integrity (see Discussion).

In summary, *lin-28* is required for normal somatic gonadal development, including uterine lumen formation, utse cell migration and proper Sp-Ut valve formation. We suggest that the abnormal Sp-Ut valve structure in *lin-28(n719)* mutants causes defects in spermathecal exit and ovulation, resulting in reduced embryo production. In addition, the embryos stalled in the spermatheca seem to suffer eggshell damage, resulting in embryonic lethality (Fig. 4E).

Embryonic lethality of *lin-28(lf)* is rescued by maternal expression of wild-type *lin-28*

We speculated that the lethality of embryos produced by *lin-28(n719)* hermaphrodites results from defects in maternal somatic gonadal morphology (which results in trapping of embryos in the spermatheca), rather than from an absence of *lin-28* function in the embryos per se. If so, then maternal expression of *lin-28* should rescue the embryonic lethality of *lin-28(n719)* homozygous embryos. To test this, we crossed *lin-28(n719)* hermaphrodites with wild-type males to obtain heterozygous mutants [*lin-28(n719)/+*], and then assessed the viability of *lin-28(n719)* homozygous self-progeny from these *lin-28(n719)/+* hermaphrodites. Viable *lin-28(n719)* homozygotes were identified by their characteristic egg-laying defective phenotype as adults. Among the self-progeny of heterozygous [*lin-28(n719)/+*] hermaphrodites, we observed a ratio of wild-type progeny [*+/+* or *lin-28(n719)/+*] to egg-laying defective progeny [*lin-28(n719)/lin-28(n719)*] of 2.89(±0.2):1 on average, which is very close to the expected 3:1 ratio for complete maternal rescue of embryonic lethality (Table 1). This finding

Development (2019) 146, dev164293. doi:10.1242/dev.164293

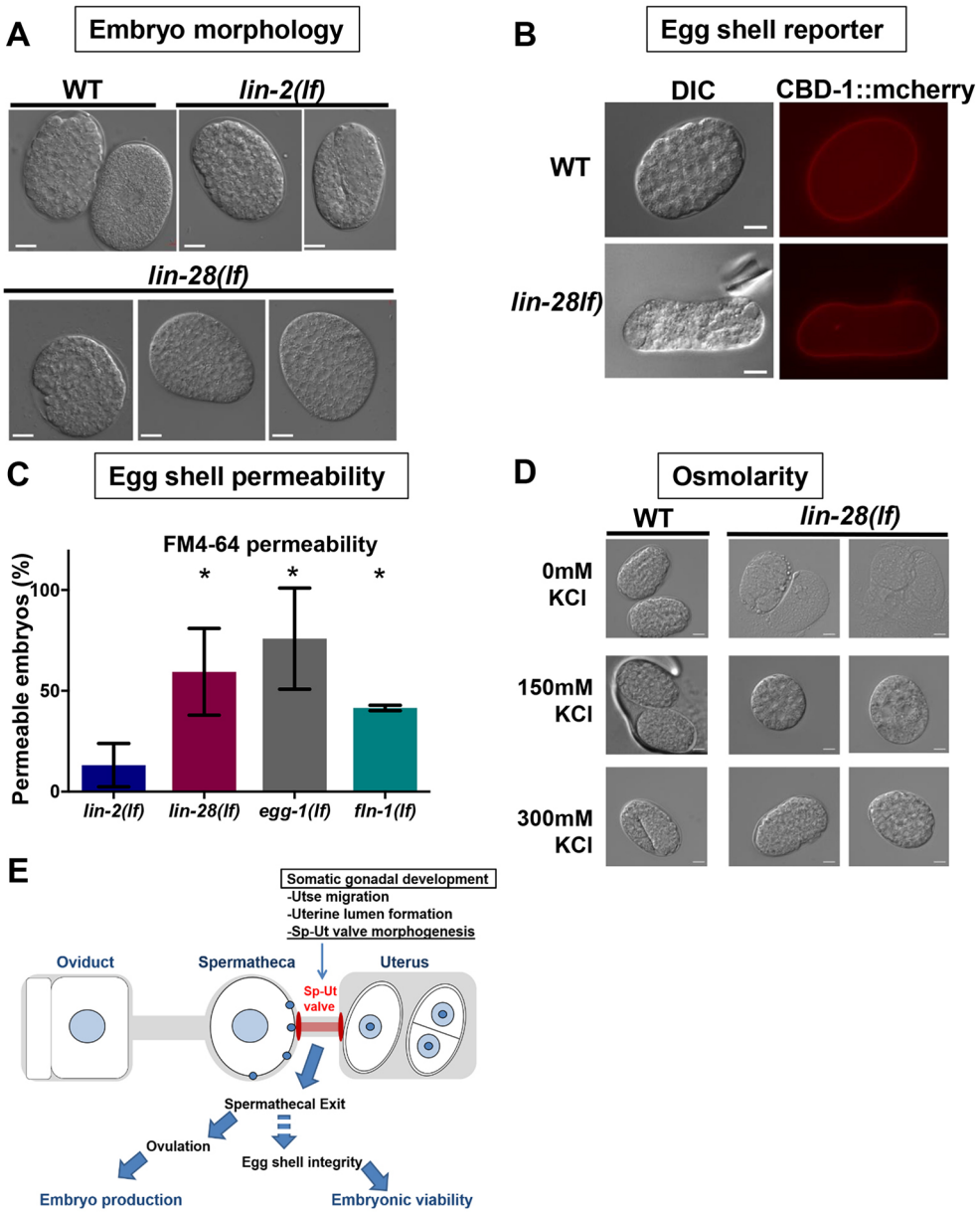

Fig. 4. *lin-28(lf)* embryos are misshapen and are defective in eggshell integrity. (A) DIC images of wild-type, *lin-2(e1309)* and *lin-28(n719)* embryos from dissected adult animals. Wild type and *lin-2(e1309)* mutants produce ovoid embryos, but *lin-28(n719)* embryos exhibit irregular shapes. (B) *cbd-1::mCherry* expression indicates that eggshells are present in *lin-28(n719)* embryos despite their misshapen morphology (lower panels). (C) Eggshell permeability of embryos produced by *lin-2(e1309)*, *lin-28(n719)*, *egg-1(tm1071)* and *fln-1(tm545)* hermaphrodites. Eggshell mutant *egg-1(tm1071)* served as a control. Embryos from *lin-28(n719)*, *fln-1(tm545)* and *egg-1(tm1071)* were more permeable to the lipophilic dye FM 4-64 than *lin-2(e1309)* embryos. Like *lin-28(n719)*, *fln-1(tm545)* hermaphrodites exhibit defects in spermathecal exit. Permeability was calculated as the percentage of permeable embryos/total embryos from dissected adult animals. Number of animals≥15 per each assay; number of independent replicate assays=3 for each strain. Data are mean±s.d. analyzed using an unpaired *t*-test compared with *lin-2(e1309)*, **P*<0.05. (D) Morphology of embryos under different osmotic conditions. *lin-28(n719)* embryos were more sensitive than wild type to low-salt conditions, indicating a lack of protection from osmotic stress. (E) Model for physiological causes of fertility defects in *lin-28(lf)* mutants. *lin-28(lf)* animals have abnormal Sp-Ut valve structure, which leads to defects in spermathecal exit and ovulation, and hence a reduced embryo production. In addition, retention of embryos in the spermatheca compromises eggshell integrity, which causes embryonic lethality.

suggests that *lin-28(n719)* embryonic lethality reflects a requirement for *lin-28* activity in the mother to enable proper development of her somatic gonad, which is required for the production of viable embryos.

Table 1. Ratio of egg laying and egg laying defective progeny from *lin-28* heterozygous mutants

lin-28(+)/lin-28(−) heterozygote number	Number of egg laying progeny	Number of egg laying defective progeny	Ratio (egg laying/egg laying defective)*
1	133	43	3.09
2	108	40	2.70
3	89	31	2.87
4	71	27	2.63
5	142	46	3.09
6	111	41	2.71
7	102	35	2.91
8	131	42	3.12

*Average ratio±s.d.=2.89±0.20.

Genes downstream of *lin-28* in developmental timing regulation also function downstream of *lin-28* in somatic gonadal morphogenesis and fertility

Functional interactions of *lin-28* with other heterochronic genes for the control of *C. elegans* hypodermal cell lineage developmental timing have been described previously (Ambros, 2011; Resnick et al., 2010) (see Fig. 5E). *lin-28* functions upstream of *lin-46* and *hbl-1* to control the timing of L2 to L3 fate transitions in hypodermal cell lineages, and *lin-28* also acts via a pathway consisting of *let-7*, *hbl-1*, *lin-41* and *lin-29* to regulate the transition from L4 fates to adult fates in the hypodermis.

To determine whether these same heterochronic genes that act downstream of *lin-28* for hypodermal cell fate timing also function in fertility and embryonic lethality, we examined those phenotypes in double mutants of the heterochronic genes (Fig. 5A-C). The number of live progeny per animal produced by the *lin-28(n719);let-7(mn112)* and *lin-28(n719);lin-29(n836)* double mutants was significantly higher than that produced by the *lin-28(n719)* mutants (Fig. 5A). In addition, the number of

Development (2019) 146, dev164293. doi:10.1242/dev.164293

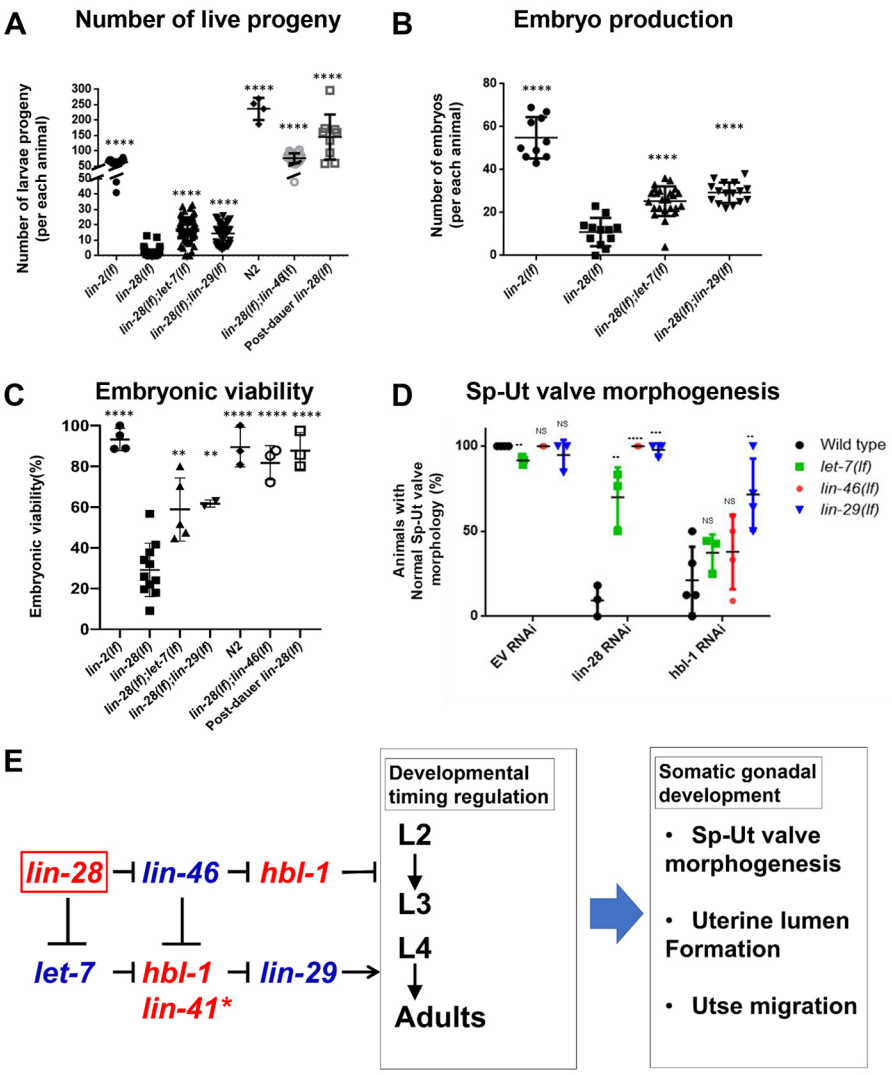

Fig. 5. Genetic epistasis analysis of *lin-28* and other heterochronic genes for effects on fertility, embryonic lethality and Sp-Ut valve morphogenesis. (A) Total number of viable larva progeny of *lin-2(e1309)*, *lin-28(n719)*, *lin-28(n719);let-7(mn112)*, *lin-28(n719);lin-29(n836)*, *lin-46(ma164);lin-28(n719)* mutants, post-dauer *lin-28(n719)* and wild type. (B) Embryo production of *lin-2(e1309)*, *lin-28(n719)*, *lin-28(n719);let-7(mn112)* and *lin-28(n719);lin-29(n836)* mutants. (C) Embryonic viability of *lin-2(e1309)*, *lin-28(n719)*, *lin-28(n719);let-7(mn112)*, *lin-28(n719);lin-29(n836)* and *lin-46(ma164);lin-28(n719)* mutants, post-dauer *lin-28(n719)* and wild type. Number of animals≥15 per each assay; each dot represents an independent replicate assay. The number of progeny of *lin-28(n719)* mutants is increased by loss of *let-7*, *lin-29* or *lin-46.* (A). Both embryo production (B) and embryo viability (C) are improved by loss of *let-7*, *lin-29* or *lin-46*. Total number of progeny and embryonic viability of *lin-28(lf)* mutants are also improved by post-dauer development (A,C). Data are mean±s.d. analyzed using an unpaired *t*-test compared with *lin-28(lf)*; NS; not significant; ***P*<0.01, *****P*<0.0001. (D) The percentage of animals with normal Sp-Ut valve core morphology, visualized by *cog-1::GFP* expression in wild type, *let-7(mn112)*, *lin-46(ma164)* and *lin-29(n836)* mutants, treated with control RNAi (EV, empty vector strain L4440), *lin-28*(RNAi) or *hbl-1*(RNAi). Wild type, *lin-46(ma164)* and *lin-29(n836)* mutants treated with L4440 empty vector RNAi rarely showed Sp-Ut valve defects. *let-7(mn112)* mutants with control RNAi showed less than 10% of Sp-Ut valve defects. *lin-28*(RNAi) treatment of wild type led to ∼95% Sp-Ut valve defects, an effect that was partially or fully suppressed by *let-7(mn112)*, *lin-46(ma164)* and *lin-29(n836). hbl-1* (RNAi) treatment of wild type also led to Sp-Ut valve defects that were rarely suppressed by *let-7(mn112)* or by *lin-46(ma164)*, or by moderately suppressed (∼70%) by *lin-29(n836)*. Number of animals≥12 per assay; each dot represents an independent replicate assay. Data are mean±s.d. analyzed using an unpaired *t*-test. Significance was calculated by comparing each mutant with wild type in each RNAi set. NS, not significant; ***P*<0.01; ****P*<0.001; *****P*<0.0001. (E) The genetic regulatory pathway model for somatic gonadal morphogenesis, derived from the results of epistasis experiments presented in Fig. 5A-D, is highly similar to the model for temporal regulation of hypodermal cell fates derived from previous studies (Ambros, 2011; Resnik et al., 2010). (See Discussion regarding the possible involvement of *lin-41* in somatic gonadal morphogenesis.) We suggest that the specification of proper hypodermal developmental timing by these genes is essential for somatic gonadal morphogenesis.

live progeny of *lin-28(n719);lin-46(ma164)* was even greater than that of *lin-2(e1309)*, because the loss of *lin-46* rescued the vulva and egg-laying defects of *lin-28(n719)* mutants. *lin-28(n719);let-7(mn112)* and *lin-28(n719);lin-29(n836)* mutants produced more embryos per animal than *lin-28(n719)* mutants (Fig. 5B) and the embryonic lethality was suppressed in these double mutants, compared with *lin-28(n719)* (Fig. 5C). The embryonic viability of *lin-28(n719);lin-46(ma164)* was similar to wild-type animals (Fig. 5C).

Consistent with the genetic epistasis observed above for fertility and embryonic viability, *lin-46(lf)*, *let-7(lf)* and *lin-29(lf)* were also epistatic to *lin-28(lf)* for somatic gonadal morphogenesis. Our RNAi knockdown experiments showed that genetic absence of *let-7*, *lin-46* or *lin-29* suppresses the Sp-Ut valve defects caused by *lin-28(RNAi)*.

Development (2019) 146, dev164293. doi:10.1242/dev.164293

hbl-1(RNAi) phenocopied the fertility phenotypes of *lin-28(n719)* mutants, including abnormal Sp-Ut valve core morphology (Fig. S7A,B). Loss of *lin-46* or *let-7* function rarely affected the Sp-Ut valve morphological defect in *hbl-1(RNAi)* animals, indicating *hbl-1* is epistatic to these genes. Finally, ∼70% of *lin-29(lf);cog-1::GFP* animals showed the wild-type Sp-Ut valve core cell morphology when *hbl-1* function was compromised (Fig. 5D). In addition, a normal uterine lumen was observed in ∼50% of *lin-28(n719);let-7(mn112)* mutants (Fig. S4D). Most *lin-28(n719); lin-29(n836)* and *lin-28(n719);lin-46(ma164)* mutants showed complete uterine lumen formation (Fig. S4E,F). Utse cell migration defects of *lin-28(lf)* mutants were also partially suppressed by loss of either *let-7* or *lin-46* (Fig. S5G-J). Overall, our findings indicate that *let-7*, *lin-46*, *hbl-1* and *lin-29* act downstream of *lin-28* for somatic gonadal development in a network configuration that is essentially identical to that previously described for the control of hypodermal cell fate timing by these same genes (Fig. 5E).

Developmental timing of hypodermal tissues and somatic gonadal tissues is discoordinated in *lin-28(lf)* mutants

Based on the above observations indicating parallels between the control of hypodermal developmental timing and somatic gonadal morphogenesis by *lin-28* mutants, we investigated whether the stage specificity of somatic gonadal developmental events might be altered in *lin-28(n719)* hermaphrodites, in analogy to their precocious hypodermal development. As a marker to monitor the expression of stage-specific programs in the somatic gonad and hypodermis, we employed *cog-1::GFP* (Palmer et al., 2002), which is expressed in the wild-type dorsal uterus and Sp-Ut valve core, beginning from late-L3/early-L4 stage (Fig. 6A). *cog-1::GFP* is also expressed in the ventral hypodermis (vulval cell lineages), beginning in the mid L4 stage, which is after the onset of *cog-1::GFP* somatic gonadal expression (Fig. 6B).

We examined whether the normal relative order of *cog-1::GFP* expression in the somatic gonad and vulva is altered in *lin-28(n719)* mutants. In *lin-28(n719)* hermaphrodites, *cog-1::GFP* expression in the vulva was observed precociously in the mid-3rd larval stage (Fig. 6D), consistent with the previously described precocious vulval cell divisions of *lin-28(lf)* mutants (Euling and Ambros, 1996). However, the onset of somatic gonadal expression of *cog-1::GFP* was normal, beginning from the late 3rd larval stage in both *lin-28(n719)* and in the wild type (Fig. 6E). Thus, the expression of *cog-1::GFP* in the vulva precedes the expression in somatic gonads in *lin-28(n719)* mutants. These data suggest that the somatic gonadal development, at least as reflected by *cog-1::GFP* expression, is not precocious in *lin-28(n719)*, despite precocious development of the hypodermis. Therefore, developmental events in hypodermal tissues and somatic gonadal tissues are temporally discoordinated in *lin-28(n719)* mutants (Fig. 6F). We hypothesize that this discord, between the precociously developing hypodermis and normally timed somatic gonad, causes abnormal somatic gonadal morphogenesis.

To investigate the hypothesis that the somatic gonadal defects of *lin-28(n719)* mutants are caused by precocious development of the hypodermis, we examined whether post-dauer development, which has been shown to suppress the precocious hypodermal development of *lin-28(n719)* (Euling and Ambros, 1995; Liu and Ambros, 1991), can also rescue *lin-28(n719)* somatic gonadal defects. We observed that after post-dauer development, *lin-28(n719)* adults exhibited restored fertility and embryonic viability, normal morphology of the Sp-Ut valve core, uterine lumen, and normal utse cell migration (Fig. 5A,C, Figs S7E, S4G, S5E and S5F). This suppression of somatic gonadal defects in *lin-28(n719)* animals by post-dauer development supports the supposition that *lin-28* acts indirectly, via downstream genes and events, to mediate normal somatic gonadal morphogenesis (Fig. 5E).

Hypodermal expression, but not somatic gonadal expression, of *lin-28* rescues somatic gonadal defects, embryonic lethality and reduced number of total progeny in *lin-28(lf)* hermaphrodites

If the somatic gonadal morphological defects of *lin-28(n719)* mutants originate from discoordination between the timing of hypodermal and somatic gonadal development, suppressing the precocious hypodermal development in *lin-28(n719)* mutants should also rescue the somatic gonadal phenotypes. To test whether *lin-28* expression specifically in the hypodermis could rescue the Sp-Ut valve morphological defects of *lin-28(n719)*, we employed Mos1-mediated single copy insertion (MosSCI) transformation to generate transgenic worms expressing *lin-28::GFP::lin-28* 3′ UTR driven by tissue-specific promotors; these included *lin-28* endogenous promoter sequences, a *dpy-7* hypodermal promoter (Gilleard et al., 1997) and an *ehn-3A* early somatic gonadal promoter (Large and Mathies, 2010). The endogenous *lin-28* promoter drives *lin-28::GFP* expression in neurons and hypodermis, where *lin-28* is known to be expressed (Moss et al., 1997). Using spinning disk microscopy, we also detected *lin-28p::lin-28::GFP* expression in Z1 and Z4 cells, which are precursors of somatic gonadal tissues (Fig. S8A,B). *dpy-7p::lin-28::GFP* was expressed in the hypodermis during the embryonic and L1 stages, and *ehn-3Ap::lin-28::GFP* expression was strongest in Z1 and Z4 from the late embryo to L1 stages (Fig. S8C,D). *lin-28::GFP* levels decreased from the L2 stage in all three strains, presumably owing to repression mediated by the *lin-28* 3′ UTR.

We crossed those MosSCI transgenic strains with *lin-28(n719); cog-1::GFP* hermaphrodites to assess the relative timing of somatic gonadal and hypodermal *cog-1::GFP* expression. *cog-1::GFP* was expressed in somatic gonadal tissues prior to the vulva in wild-type animals, whereas *cog-1::GFP* expression in the vulva was precocious in the *lin-28(n719)* mutants (Figs 6 and 7A,B). *lin-28* expression via its endogenous promoter (*lin-28p::lin-28::GFP::lin-28* 3′UTR) restored the normal relative timing of somatic gonadal and hypodermal *cog-1::GFP* expression in *lin-28(n719)* mutants (Fig. 7C). Similarly, in *dpy-7p::lin-28::GFP;lin-28(n719);cog-1::GFP* animals, *cog-1::GFP* expression in the vulva occurred at the normal time, following somatic gonadal expression. Thus, hypodermal expression of *lin-28* efficiently rescues precocious hypodermal development of *lin-28(n719)* (Fig. 7D). By contrast, somatic gonadal expression of *lin-28* via the *ehn-3Ap::lin-28::GFP* transgene did not rescue the precocious expression of hypodermal *cog-1::GFP* in *lin-28(n719)* mutants (Fig. 7E). These results are consistent with cell-intrinsic activity of *lin-28* in the hypodermis to control hypodermal developmental timing.

Does hypodermal expression of *lin-28* also rescue the somatic gonadal morphogenesis defects of *lin-28(n719)* hermaphrodites? Indeed, *dpy-7p::lin-28::GFP* did rescue wild-type morphology of the Sp-Ut valve core in *lin-28(n719)*, (Fig. 7F,H,I), normal uterine lumen formation (Fig. S4I) and normal utse cell migration (Fig. S5M,N). By contrast, somatic gonadal *lin-28* expression did not rescue *lin-28(n719)* somatic gonadal defects (Fig. 7G,J, Figs S4J, S4K, S5O and S5P).

We also performed mosaic analysis to investigate whether hypodermal expression of *lin-28* is necessary and sufficient for somatic gonadal morphogenesis (Yochem and Herman, 2003).

Development (2019) 146, dev164293. doi:10.1242/dev.164293

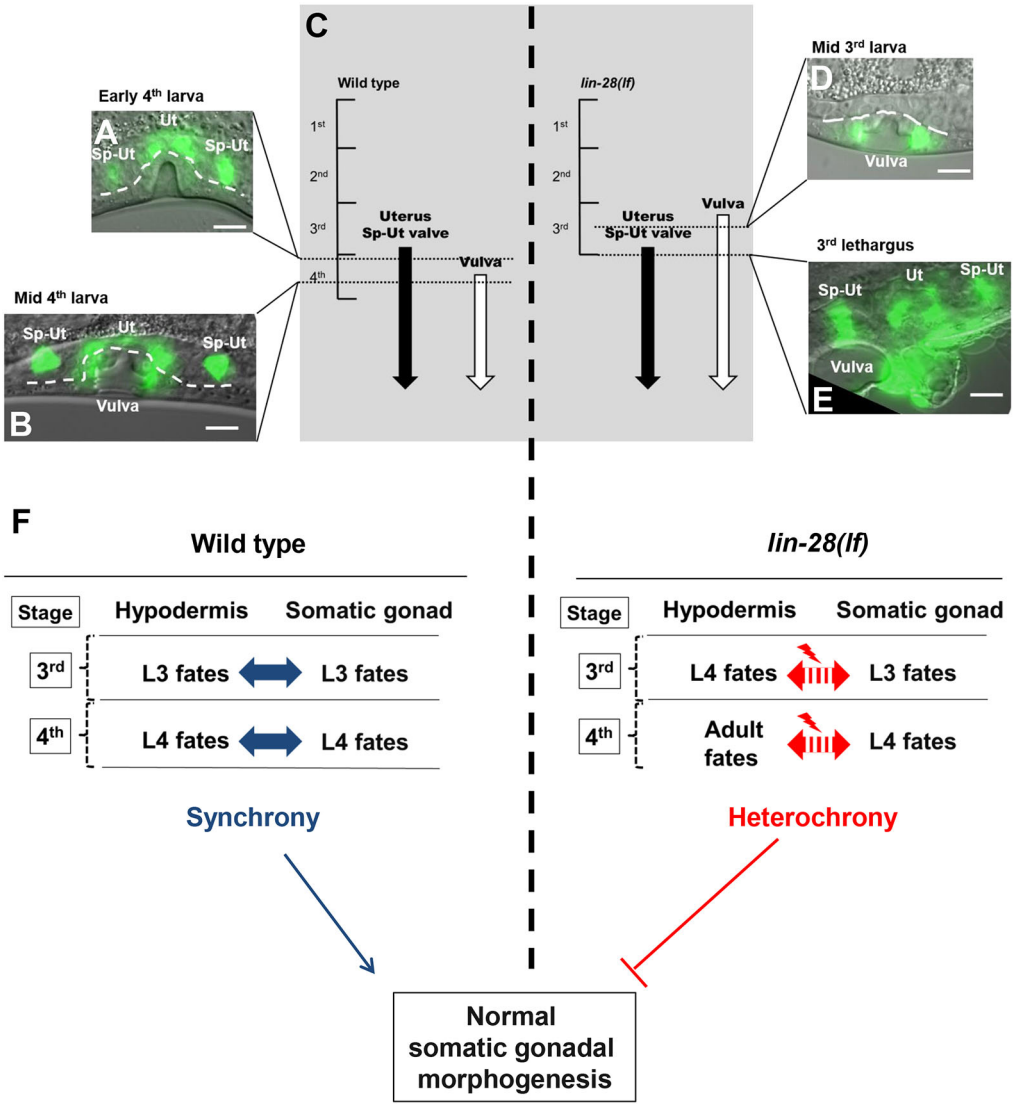

Fig. 6. Heterochronic development of the hypodermis, relative to the somatic gonad, in *lin-28(lf)* hermaphrodites. (A,B,D,E) *cog-1::GFP* expression patterns in wild type and *lin-28(n719)* hermaphrodites at indicated developmental stages. The temporal order of the onset of *cog-1::GFP* expression in the somatic gonad and vulva is reversed in *lin-28(lf)* compared with the wild type. *cog-1::GFP* is expressed in both somatic gonadal tissues (uterus and Sp-Ut valve) and hypodermal tissue (vulva). The timing of expression in wild type and *lin-28(n719)* mutants is summarized in C. In the wild type, *cog-1::GFP* expression in somatic gonadal tissues first appears during the late 3rd larval stage and is not yet apparent in the vulva at the early 4th larval stage (A). Vulval expression of *cog-1::GFP* starts at the middle of the 4th larval stage (B). In *lin-28(n719)* mutants, vulval expression of *cog-1::GFP* occurs precociously in the middle of the 3rd larval stage (D), whereas somatic gonadal expression of *cog-1::GFP* starts at the normal time, in the late 3rd larval stage (E). Both vulval and somatic gonadal expression are detected at 3rd lethargus (E). (F) Model for the importance of *lin-28* activity for somatic gonadal development. In wild-type animals, timing of hypodermis development and somatic gonadal development are synchronized. In *lin-28(lf)* mutants, hypodermal development happens precociously, whereas somatic gonadal development does not, resulting in heterochronic development between two tissues. We suggest this heterochrony causes somatic gonadal morphogenesis defects. Scale bars: 10 µm.

We constructed *lin-28(n719);cog-1::GFP* strains with an extrachromosomal transgenic array containing a *lin-28* expression vector and a *sur-5::GFP* plasmid as a reporter for the array. Twelve mosaic animals that completely lost the extra-chromosomal array in the Z1 and Z4 lineages, but not in hypodermal lineage, all showed wild-type Sp-Ut valve core morphology at the young adult stage (Fig. 8A, Fig. S9B). For seven out of eight mosaic animals in which *sur-5::GFP* was undetectable in the hypodermis, but clearly expressed in the Z1 and Z4 lineages, wild-type Sp-Ut valve core morphology was not observed (Fig. 8B, Fig. S9C). This suggests that loss of *lin-28* expression in hypodermal tissues, but not in somatic gonadal tissues, is correlated with abnormal Sp-Ut valve morphogenesis (Fig. 8C, Fig. S9).

Because the hypodermal expression of *lin-28* suppresses the morphological defects of the somatic gonad in *lin-28(n719)* mutants (Fig. 7), we investigated whether embryonic lethality and fertility defects were accordingly rescued, as would be expected. Expression of either *lin-28p::lin-28::GFP* or *dpy-7p::lin-28::GFP* restored the embryo viability of *lin-28(n719)* progeny, whereas *ehn-3Ap::lin-28::GFP* expression did not restore viability of *lin-28(n719)* progeny (Fig. 9A).

Interestingly, although the total number of live progeny was greater for the *dpy-7p::lin-28::GFP;lin-28(n719)* strain than for the *lin-28(n719)* mutants, the number of progeny was comparable with the wild type in only ∼15% of animals; the other ∼85% of animals produced fewer than 20 progeny at 25°C. In addition, the

Development (2019) 146, dev164293. doi:10.1242/dev.164293

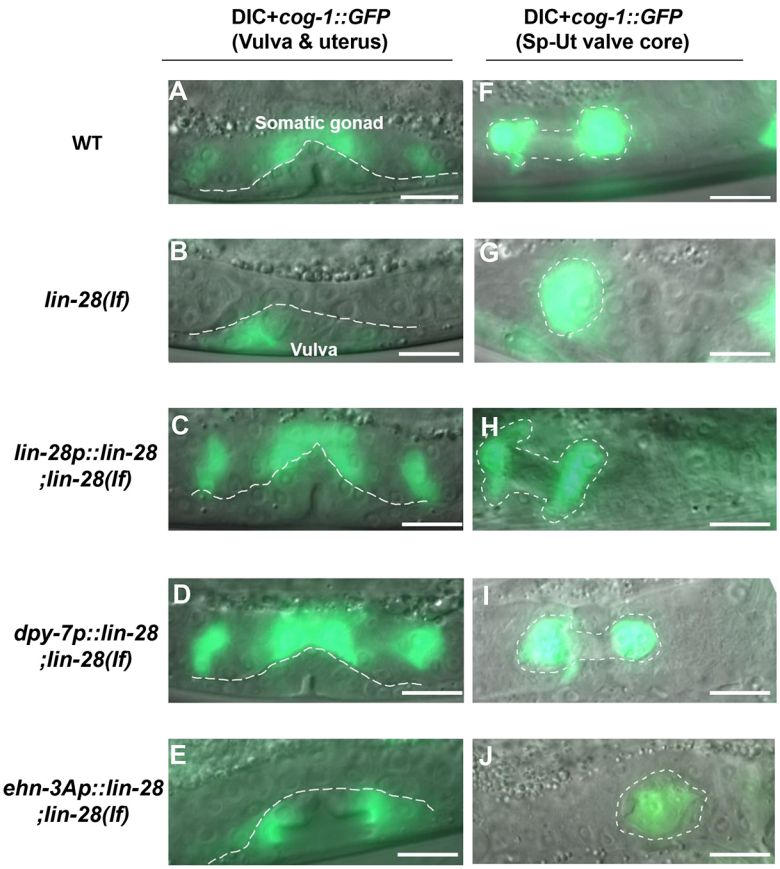

Fig. 7. Hypodermal expression of *lin-28* rescues developmental timing defects and Sp-Ut valve morphogenesis in *lin-28(lf)* mutants. *cog-1::GFP* expression in the somatic gonad and vulva (below the dashed line) in late 3rd or early 4th larval stage hermaphrodites (A-E), or in the Sp-Ut valve (outlined) in adult or 4th stage hermaphrodites (F-J), of the wild type (A,F), *lin-28(lf)* (B,G) and *lin-28(lf)*, with *lin-28* expression driven by various promoters (C-E,H-J). *dpy-7p* (D,I) is a hypodermal-specific promoter (Gilleard et al., 1997) and *ehn-3Ap* (E,J) is an early somatic gonadal-specific promoter (Large and Mathies, 2010). In these experiments, the promoter-driven *lin-28* transgene (C-E,H-J) is also tagged with GFP, but *lin-28::GFP* expression is not detectable at these stages, so all the GFP signal shown here corresponds to *cog-1::GFP*. *lin-28p::lin-28::GFP;lin-28(n719)* (C) and *dpy-7p::lin-28::GFP;lin-28(n719)* (D) express *cog-1::GFP* in the somatic gonad earlier than in the vulva, as in wild type (A). In contrast, both *lin-28(n719)* mutants (B) and *ehn-3Ap::lin-28::GFP;lin-28(n719)* (E) express *cog-1::GFP* precociously in the vulva. Eighty-three percent of *lin-28p::lin-28::GFP;lin-28(n719)* (H) and 95% of *dpy-7p::lin-28::GFP;lin-28(n719)* (I) animals exhibit the Sp-Ut core dumbbell structure observed in wild type (F). However, the Sp-Ut valve core structure remains as a single lobe shape in both *ehn-3Ap::lin-28::GFP; lin-28(n719)* (J) and *lin-28(n719)* (G) animals (94% and 98%, respectively). These data suggest that hypodermal expression of *lin-28* is sufficient to rescue heterochronic development (A-E) and abnormal Sp-Ut valve core morphogenesis (F-J) in *lin-28(n719)* mutants, but somatic gonadal expression of *lin-28* cannot rescue either defect. Scale bars: 10 µm.

dpy-7p::lin-28::GFP transgene in the wild-type background led to a similarly reduced number of progeny, indicating that the expression of *dpy-7p::lin-28::GFP* alone is sufficient to reduce fertility, apparently by impairing egg-laying (Fig. 9C). In contrast, somatic gonadal promoter-driven *lin-28::GFP* expression did not affect the number of progeny produced by *lin-28(n719)* hermaphrodites (Fig. 9B).

DISCUSSION

C. elegans lin-28(lf) hermaphrodites exhibit a dramatic reduction in fertility, in excess of what would be expected as a simple consequence of their vulval morphogenesis defects. In principle, it is possible that *lin-28* could promote fertility entirely via a germline-specific activity, analogous to the demonstrated role of mammalian Lin28 in promoting pluripotency and stem cell proliferation (Yu et al., 2007; Zhang et al., 2016). Indeed, *lin-28* has been reported to regulate the germ cell pool size in mice and in *C. elegans* hermaphrodites (Shinoda et al., 2013; Wang et al., 2017). However, the reported effects on germ cell pool size in *C. elegans*, after germline knockdown of *lin-28*, did not include substantially reduced fertility (Wang et al., 2017). Our results suggest that the reduced fertility of *lin-28(lf)* hermaphrodites is caused by fertility-promoting activities of *lin-28* outside the germline, i.e. within somatic cell lineages of the gonad and/or other tissues. Other examples in which *lin-28* controls the development of reproductive tissues other than germ cells have been reported in flies and mice. The *Drosophila* egg chamber is fused abnormally early in *lin-28*-null mutants, and the development of mice vaginal openings is delayed in *lin-28a* transgenic mice (Stratoulias et al., 2014; Zhu et al., 2010).

Here, we have investigated the somatic function of *lin-28* in promoting *C. elegans* hermaphrodite fertility. Our results show that *lin-28* is required for the completion of certain somatic gonadal morphogenetic events, specifically, the enlargement of the uterine lumen, the migration of utse nuclei and the extension of the Sp-Ut valve core, and that these somatic gonadal morphogenesis defects likely underlie the reduced fertility of *lin-28(lf)* hermaphrodites. In particular, the abnormal Sp-Ut valve of *lin-28(lf)* animals has a potent impact on fertility by preventing fertilized embryos from entering the uterus, thereby inhibiting ovulation and resulting in reduced embryo production.

We also found compromised eggshell integrity in *lin-28(lf)* mutants, which negatively affects embryonic viability, similar to other eggshell defective mutants (Johnston et al., 2006, 2010; Maruyama et al., 2007). Moreover, we found that another spermathecal exit mutant *fln-1(lf)* has eggshell-defective phenotypes similar to *lin-28(lf)* (Fig. 4C), suggesting a causal link between spermathecal retention and loss of eggshell integrity. We speculate that physical damage to the eggshells may occur when the embryos are trapped in the spermatheca. Interestingly, deficiency of *cbd-1*, an essential component of the *C. elegans* eggshell, leads to pinched-off embryos reflecting incomplete spermathecal exit (Johnston et al., 2010). This suggests that damage to the eggshell of embryos lingering too long in the spermatheca could further aggravate an underlying spermathecal exit defect. Further research is needed to clarify the relationship between spermathecal exit and eggshell integrity.

Our results point to a close coupling between the hypodermal and somatic gonadal phenotypes in *lin-28(lf)* mutants. First, we found that a very similar configuration of the known heterochronic genes mediates the effects of *lin-28(lf)* on hypodermal developmental timing and on somatic gonadal morphogenesis (Fig. 5E). The exception is *lin-41*; we could not find evidence that *lin-41*, a

Development (2019) 146, dev164293. doi:10.1242/dev.164293

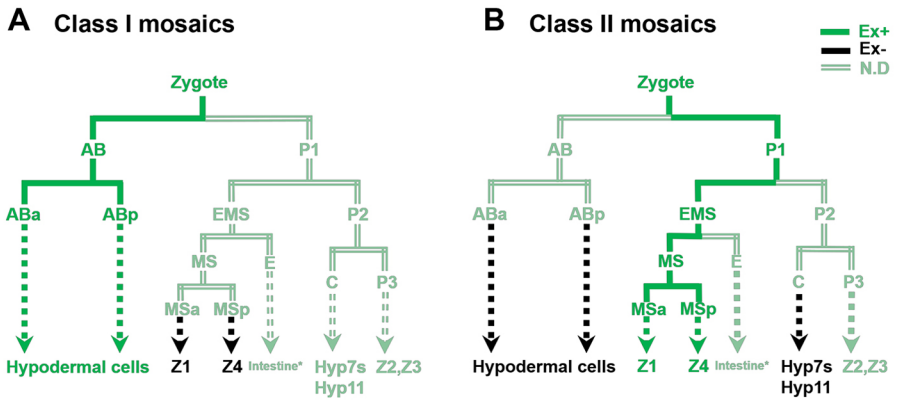

C

Class	LIN-28 expression	Sp-Ut valve morphology	
		Normal	Abnormal
Ex+ Control	Hyp+ Somatic gonad+	43	1
Class I Mosaic	Hyp+ Somatic gonad-	12	0
Class II Mosaic	Hyp- Somatic gonad+	1	7
Ex- Control	Hyp- Somatic gonad-	2	28

n.s
n.s
****
****
****

Fig. 8. *lin-28(lf)* mosaic analysis for Sp-Ut valve morphogenesis. (A,B) Summary of mosaic expression patterns of *sur-5::GFP* in VT3884 animals where the extrachromosomal array maEx265[*sur-5::GFP*; *lin-28p::lin-28::GFP*] was lost either (A) in a precursor of Z1 and Z4 or (B) in hypodermal lineages (the AB lineage and probably also in P2 or C). (See Fig. S9 for more detailed analysis of individual mosaic animals and non-mosaic controls.) The observed *sur-5::GFP* expression pattern for these two classes of mosaic animals are color coded: dark green, confirmed *sur-5::GFP* expression; black, confirmed absence of *sur-5::GFP* expression; light green, *sur-5::GFP* expression not determined. Dotted lines represent multiple cell divisions not shown in these abbreviated cell lineage diagrams. (Expression in the E lineage was determined in some mosaic animals, but was not relevant to Sp-Ut valve core morphogenesis; see Fig. S9B,C.) (C) Summary of the phenotypes exhibited by class I and class II mosaic animals and non-mosaic controls. Presence of wild-type Sp-Ut valve core morphology was determined in mosaic animals (A,B) as well as in the control animals, which contained or completely lost extrachromosomal arrays in both hypodermal and somatic gonadal lineages (Fig. S9A,D). Data were analyzed using a Chi-square test. n.s, not significant; ****P<0.0001.

downstream target of *let-7* for hypodermal developmental timing (Slack et al., 2000), is involved in Sp-Ut valve core morphogenesis. The *lin-41*(RNAi) animals displayed a superficially normal dumbbell-shaped Sp-Ut valve, albeit somewhat smaller than the wild-type valve (Fig. S7C). This result may reflect either an insufficient knockdown of *lin-41* by RNAi in these experiments, or that *lin-41* does not participate in somatic gonadal development. In the latter event, *hbl-1* would appear to function as a main downstream target of *let-7* in somatic gonadal morphogenesis.

Our second finding indicating a link between *lin-28(lf)* hypodermal and somatic gonadal phenotypes is the observation that post-dauer development suppresses both the hypodermal and the somatic gonadal developmental defects of *lin-28(lf)* hermaphrodites. This result in particular accentuates the fact that the somatic gonadal defects of *lin-28(lf)* do not reflect a direct role of *lin-28* in somatic gonadal development per se; rather, somatic gonadal morphogenesis fails in *lin-28* mutants as an indirect consequence of precocious development. Consistent with this idea, another precocious mutant, *lin-14(lf)* (Ambros and Horvitz, 1984), showed similar Sp-Ut valve defects to *lin-28(lf)* mutants (Fig. S7D).

Importantly, we did not find evidence for precocious development of somatic gonadal events in *lin-28(lf)*. In particular, we observed that the timing of the onset of expression of certain fluorescent markers of L3 and L4 somatic gonadal developmental events was not altered in *lin-28(lf)*, even though subsequent morphogenesis failed. Assuming that the somatic gonad and the hypodermis each has its own developmental clock, it would appear that the hypodermal developmental clock of *lin-28(lf)* mutants is accelerated, whereas the somatic gonadal developmental clock runs normally, resulting in discoordination of developmental timing between the two tissues during the L3 and L4 stages (Fig. 6F). We propose that it is this temporal discord between the accelerated hypodermis, and the normally scheduled somatic gonad, that results in failure of somatic gonadal morphogenesis.

The apparent absence of precocious development of the somatic gonad of *lin-28(lf)* animals suggests that *lin-28* may affect somatic gonadal morphogenesis cell non-autonomously, by controlling one or more signals from the hypodermis to the somatic gonad. In strong support for this model, we found that expression of *lin-28* specifically in the hypodermis could rescue the somatic gonadal developmental defects of *lin-28(lf)* mutants. Conversely, expression of *lin-28* specifically in the somatic gonadal precursor lineage did not rescue any *lin-28(lf)* phenotypes. Based on these observations, we propose that the principal function of *lin-28* with regards to somatic gonadal development is to act within the hypodermis to specify a schedule of hypodermal events that is properly coordinated with a corresponding schedule of somatic gonadal developmental events. Apparently, normal somatic gonadal morphogenesis requires a coordination between the hypodermis and the somatic gonad during the L3 and/or L4 stages.

By what mechanisms could hypodermal activity of *lin-28* regulate the development of a different tissue? There are precedents in *C. elegans* for cell non-autonomous developmental signals originating from the hypodermis. A recent study showed that heterochronic genes acting in the hypodermis can modulate mTORC2 signaling in the intestine (Dowen et al., 2016). In another example, it has been reported that migration of the hermaphrodite-specific neurons and arborization of sensory neurons are regulated by hypodermal expression of the microRNA *mir-79* and MNR-1/menorin, respectively (Pedersen et al., 2013; Salzberg et al., 2013).

Development (2019) 146, dev164293. doi:10.1242/dev.164293

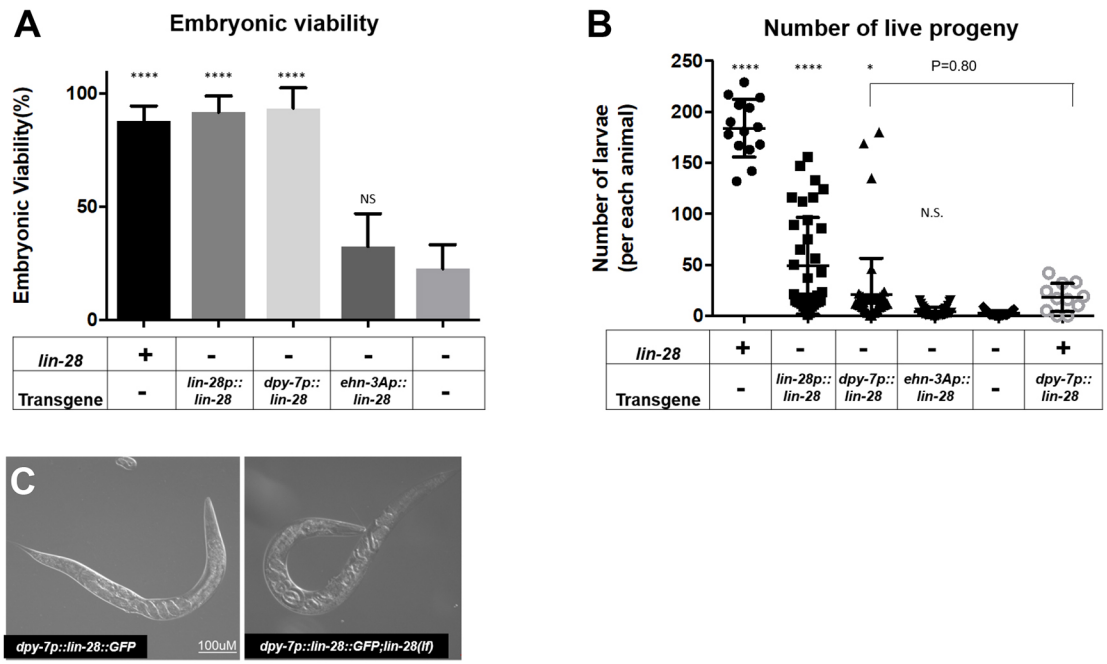

Fig. 9. Hypodermal expression of *lin-28* enhances embryonic viability and number of progeny of *lin-28(lf)* mutants. (A) Embryonic viability of *lin-28p::lin-28::GFP;lin-28(n719)* and *dpy-7p::lin-28::GFP;lin-28(n719)* are restored to a level similar to that in wild type. However, expression of *ehn-3Ap::lin-28::GFP* does not enhance the viability of *lin-28(n719)* embryos. Number of animals≥15 per each assay; number of independent replicate assays=4 for *lin-28(n719)*, 3 for all other strains. (B) The number of live larva progeny is increased in *lin-28p::lin-28::GFP;lin-28(n719)* (*n*=36) and slightly enhanced in *dpy-7p::lin-28::GFP;lin-28(n719)* (*n*=53) compared with *lin-28(n719)* mutants (*n*=25). Progeny numbers for *dpy-7p::lin-28::GFP* insertional lines without *lin-28(n719)* (*n*=11) are similar to those of *dpy-7p::lin-28::GFP;lin-28(n719)* (*P*=0.80), suggesting that expression of *dpy-7p::lin-28::GFP* induces fertility defects regardless of *lin-28(n719)*. Progeny numbers for *ehn-3Ap::lin-28::GFP;lin-28(n719)* (*n*=40) are similar to those of *lin-28(n719)* mutants. Data are mean±s.d. analyzed using an unpaired *t*-test compared with *lin-28(lf)*. N.S., not significant; **P*<0.05, *****P*<0.0001. (C) Embryos of *dpy-7p::lin-28::GFP* (left) and *dpy-7p::lin-28::GFP;lin-28(n719)* (right) are trapped inside adult hermaphrodites, indicating that defective egg laying is a cause of the reduced fertility in these animals. Scale bar: 100 µm.

Hypodermal glycosylated cell surface molecules or signaling cell-adhesion molecules are key downstream factors for neuronal morphogenesis in each case, implying this nonautonomous signaling may require physical contact with other tissues.

Indeed, seam cells in the hypodermis become physically connected to the utse of *C. elegans* hermaphrodites. The connection between these two tissues is thought to be formed during the mid to late L4 stages in wild-type animals (Newman et al., 1996). The precocious hypodermal maturation in *lin-28(lf)* animals might cause this connection to be formed aberrantly, or not at all. Alternatively, the reduced number of seam cells in *lin-28(lf)* mutants may alter positioning of seam cells in the hypodermis, disrupting the normal connection between seam cells and the utse. However, there is evidence that utse defects may not necessarily be associated with Sp-Ut valve abnormality. *lin-29* expression in the anchor cell induces signals for utse precursor cells to adopt utse fates, and *lin-29(lf)* mutants do not form a proper utse (Newman et al., 2000). However, loss of *lin-29* does not cause any detectable abnormality in Sp-Ut valve core morphology (Fig. 5D). Nevertheless, it will be interesting to examine whether the physical connection between the hypodermal seam and gonadal utse is formed properly in *lin-28(lf)* hermaphrodites.

It is striking that *lin-28(lf)* mutants exhibit defects in the final stages of morphogenesis in at least three distinct somatic gonadal structures: extension of the Sp-Ut valve core, positioning of the uterine seam cell nuclei and expansion of the lumen of the uterus. As all three of these defects are highly penetrant in *lin-28(lf)*, and are coordinately rescued by appropriate *lin-28*-expressing transgenes, we were not able to determine whether these defects are expressed independently, or whether, for example, one of them is the primary defect that is linked to hypodermal developmental timing and the other defects are secondarily precipitated by the first. Further research is needed to identify any cause-effect relationships between utse cell migration, Sp-Ut valve morphogenesis and uterine lumen formation.

Overall, our studies of *lin-28* in the context of *C. elegans* reproductive system development provides an informative model for exploring fundamental principles of multicellular development, including how the generation of organized cellular complexity requires precise temporal coordination of events across interacting tissues. Our findings exemplify how a cell-intrinsic developmental timing program can be required not only cell-autonomously to specify temporal cell fates, but also to control cell-nonautonomous signaling that is crucial for proper development of interacting tissues. Our identification of cell non-autonomous hypodermis-to-gonad developmental signaling controlled by *lin-28* and the heterochronic pathway should set the stage for future studies addressing the identity and potential evolutionary conservation of the molecular components of the downstream signal(s).

MATERIALS AND METHODS

Culture of *C. elegans* strains

C. elegans wild-type (strain N2) and mutant strains (listed in Table S1) were grown and maintained (at 25°C unless otherwise noted) on nematode growth media (NGM) agar plates seeded with *E. coli* (strain HB101). A list of genotyping primers for allele confirmation can be found in Table S2. Synchronized populations of larvae at defined developmental stages were obtained as previously described (Stiernagle, 2006). Briefly, embryos were collected using 1.2% (v/v) sodium hypochlorite and 0.5 N NaOH, washed

Development (2019) 146, dev164293. doi:10.1242/dev.164293

with M9 buffer and incubated in M9 buffer overnight at 20°C, placed on NGM plates seeded with HB101, incubated for defined lengths of time at 20°C or 25°C, and developmental stage was assessed by DIC microscopy of a sample of worms from the population (Byerly et al., 1976).

Microscopy

For DIC and fluorescence microscopy, worms were anesthetized with 0.2 mM levamisol and mounted on 2% agarose pads. All images, except the following, were obtained using a Zeiss Axiocam 503 mono: Fig. S2 (Leica DM 5500Q confocal microscopy) and Fig. S8 [3i (Intelligent Imaging Innovations) Everest spinning disk confocal microscopy]. The supplementary movies were captured using a Zeiss Axiocam 503 mono. For gonad DAPI staining, hermaphrodites were cut with a syringe needle and the extruded gonads were fixed with 95% ethanol. After washing twice with M9, the dissected gonads were incubated with 4′6′-diamidino-2-phenylindole solution (100 ng/ml) for 10 min in a humidified chamber and washed again with M9 (modified from Shaham, 2005).

RNAi

RNAi by feeding worms with *E. coli*-expressing double-stranded RNA was conducted as previously described (Conte et al., 2015). HT115 bacterial RNAi strains (*lin-28*, *hbl-1*, *lin-29*, *lin-46*) and an empty vector strain (L4440) from the Ahringer library were used (Kamath and Ahringer, 2003).

Analysis of fertility and embryonic viability

Individual young adult hermaphrodites were placed, one per plate, on NGM plates seeded with HB101, and the number of live progeny from each hermaphrodite was counted ∼3-4 days later. To determine embryo viability, gravid adult hermaphrodites were dissected with a syringe, and the released embryos were collected and transferred to NGM plates seeded with HB101. The total number of embryos was counted immediately and, after 36 h incubation at 25°C, the number of live animals was counted. Viability was calculated as (number of live animals)/(total number of embryos seeded)×100%.

Eggshell integrity

Eggshell permeability was assessed using FM 4-64 dye (Sigma, T13320), as described previously (Johnston et al., 2006). Briefly, embryos were dissected from gravid hermaphrodites in 150 mM KCl with 30 µM of FM4-64, and the proportion of embryos infiltrated by FM4-64 was measured using fluorescence microscopy.

Estimating the duration of spermathecal transit

Wild-type and *lin-28(lf)* hermaphrodites containing a spermathecal GFP reporter (strains DZ325 and VT2930, respectively) were examined in the fluorescence dissecting microscope to identify worms that had not yet undergone their first ovulation event; these animals were placed individually on seeded NGM plates. Each animal was then observed every 20 min to check for the occurrence of ovulation (evidenced by an embryo surrounded by expanded fluorescent spermathecal tissue), and/or subsequent spermathecal exit (evidenced by the embryo located in the region of the uterus and adjacent to compacted fluorescent spermathecal tissue). When an animal was first observed to contain a spermathecal-resident embryo, spermathecal entry was scored as having occurred within the previous 20 min. Likewise, if a previously spermathecal-resident embryo was observed to have exited the spermatheca, the time of spermathecal exit was scored as occurring within the previous 20 min. The maximum duration of spermathecal transit was estimated for each embryo in terms of multiples of 20 min, based on the number of 20-min intervals that encompassed spermathecal entry and spermathecal exit. For animals in which ovulation and spermathecal exit had both occurred within the previous 20 min, we estimated the maximum duration of spermathecal transit for that embryo as 20 min.

Construction of plasmids

To generate transgenic strains containing tissue-specific promoters driving *lin-28::GFP*, we removed the sequence between the first exon and second exon (I:8409341-I:8410415) of *lin-28a* to prevent the sequence from serving as an endogenous promoter (Moss et al., 1997). GFP sequences were adapted from XW12 (Wei et al., 2012) and were fused in frame to the C terminus of *lin-28*-coding sequence. The primers used for the overlapping PCRs for these procedures are listed in Table S2. We used Gateway Technology (Invitrogen, 12535-019) to construct transgenic vectors. *lin-28::GFP* was cloned into the gateway entry vector pDONR P2P3 by BP reaction. In addition, the promoter regions of *enh-3A*, *lin-28* and *dpy-7* were cloned into pDONR P4P1r by BP reaction. *lin-28* 3′UTR was cloned into pDONR P2rP3. LR reactions of these three entry vectors with pCJF150 yielded final vectors containing the following transgenes for injection: pSW40(*lin-28p*), pSW42(*ehn-3Ap*) and pSW43(*dpy-7p*). The sequences for all primers used in this procedure can be found in Table S2 and the maps of pSW40, pSW42 and pSW43 can be found in Fig. S10.

Generation of MosSCI transgenic lines

MosSCI single-copy insertions (into the *ttTi5605* Mos1 allele, near the center of chromosome II) were obtained using the protocol previously described on the 'wormbuilder' website (www.wormbuilder.org/). For each plasmid construct, MosSCI transformation was generally conducted using the direct injection approach (Frøkjær-Jensen et al., 2012), and also using the approach employing extrachromosomal array intermediates and ivermectin selection for insertion (Shirayama et al., 2012). To prepare plasmids for injection, the following plasmids were purified using a midiprep kit (Qiagen, 12143): pSW40, pSW42, PSW43, pCFJ601 (*eft-3p*::transposase), pMA122 (*hspp*::peel-1), pGH8 (*rab-3p*::mCherry), pCFJ90 (*myo-2p*::mCherry), pCFJ104 (*myo-3p*::mCherry), pJL44 (*hsp-16.48p*::MosTase::glh-2 3′UTR), pCCM416 (*myo-2p*::avr-15) and pRF4 [*rol-6(su1006)*]. For the direct injection method, injection mixtures consisted of pCFJ601 (50 ng/µl), pMA122 (10 ng/µl), pGH8 (10 ng/µl), pCFJ90 (2.5 ng/µl), pCFJ104 (5 ng/µl) and one of the transgene-containing plasmids [pSW40, pSW42 or pSW43 (25 ng/µl)]; the mixture was injected into EG4322 hermaphrodites and injected animals were placed singly onto NGM plates seeded with HB101. Following ∼7-10 days of incubation at 25°C, cultures were heat-shocked (35°C, 1 h) to kill any worms with an extrachromosomal array and surviving animals were cloned. After allowing them to produce progeny, worms are genotyped to identify single copy transgene inserted strains. For the approach using ivermectin selection, we injected a mixture of pJL44 (50 ng/µl), pCCM416 (50 ng/µl) and pRF4 (50 ng/µl) with one of pSW40, pSW42 or pSW43 (15 ng/µl) into WM186 hermaphrodites. After allowing the progeny of injected animals to grow for multiple generations, they were heat-shocked (35°C, 1 h) to induce heat shock promoter-driven transposase expression from extra chromosomal arrays, and individual single-copy transgene-inserted strains were selected by invermectin resistance (10 ng/ml) against extrachromosomal arrays. We obtained VT3702 by the direct injection method, and VT3486 and VT3392 by the extrachromosomal array intermediate method. We crossed those strains to VT2929 to obtain VT3703, VT3517 and VT3516 (Table S1).

Mosaic analysis

A transgenic strain carrying an extrachromosomal array expressing wild-type *lin-28* and *sur-5::GFP* (VT3884: *lin-28(n719)*; *syIs63[cog-1::GFP]*; *maEx265[lin-28(+); sur-5::GFP]*), was generated by injection of VT2929 with a mixture of plasmids pSW40 (20 µg/ml) and pTG96 (100 µg/ml) (Yochem et al., 1998). Populations of VT3884 animals at the 4th stage or young adult stage were screened using fluorescence microscopy to identify animals with either of two classes of mosaic patterns of *sur-5::GFP* expression (Fig. 8A,B): Class I, absence of *sur-5::GFP* in Z1 and Z4, with *sur-5::GFP* expression retained in the hypodermis (consistent with loss of the extrachromosomal array in a precursor of Z1 and Z4, with retention of the array at least in the AB lineage); class II, absence of detectable *sur-5::GFP* in the hypodermis, along with *sur-5::GFP* expression retained in Z1 and Z4 (corresponding to presumed loss of the extrachromosomal array in the AB lineage, and a second loss of the array in the P2 or C blastomere). Sp-Ut valve core morphology was scored for each animal based on *cog-1::GFP* expression.

Acknowledgements

We thank members of the Ambros Lab, Anna Zinovyeva (Kansas State University), Katherine McJunkin (NIH) and Yoshiki Andachi (National Institute of Genetics)

for helpful discussions and critical comments about this project. We also thank Erin Cram (Northeastern University) and Anna Allen (Howard University) for sharing strains, Kang Shen (Stanford University) and Sean Ryder (University of Massachusetts Medical School) for sharing plasmids, and Amy Walker, Craig Mello and Michael Gorzyca (University of Massachusetts Medical School) for help with microscopy. We thank Wormbase and the Caenorhabditis Genetics Center for data resources and strains. The NIH had no role in study design, data collection and interpretation, or the decision to submit the work for publication.

Competing interests

The authors declare no competing or financial interests.

Author contributions

Conceptualization: S.C., V.A.; Methodology: S.C., V.A.; Validation: S.C.; Formal analysis: S.C.; Investigation: S.C.; Resources: V.A.; Data curation: S.C.; Writing - original draft: S.C.; Writing - review & editing: S.C., V.A.; Visualization: S.C.; Supervision: V.A.; Project administration: V.A.; Funding acquisition: V.A.

Funding

This work was funded by the National Institutes of Health (R01GM104904-04 and R01GM034028-32 to V.A.). Deposited in PMC for release after 12 months.

Supplementary information

Supplementary information available online at
http://dev.biologists.org/lookup/doi/10.1242/dev.164293.supplemental

References

Abbott, A. L., Alvarez-Saavedra, E., Miska, E. A., Lau, N. C., Bartel, D. P., Horvitz, H. R. and Ambros, V. (2005). The let-7 microRNA family members mir-48, mir-84, and mir-241 function together to regulate developmental timing in caenorhabditis elegans. *Dev. Cell* **9**, 403-414.

Allen, A. K., Nesmith, J. E. and Golden, A. (2014). An RNAi-based suppressor screen identifies interactors of the Myt1 ortholog of Caenorhabditis elegans. *G3* **4**, 2329-2343.

Ambros, V. (2011). MicroRNAs and developmental timing. *Curr. Opin. Genet. Dev.* **21**, 511-517.

Ambros, V. and Horvitz, H. (1984). Heterochronic mutants of the nematode Caenorhabditis elegans. *Science* **226**, 409-416.

Ambros, V. and Horvitz, H. R. (1987). The lin-14 locus of Caenorhabditis elegans controls the time of expression of specific postembryonic developmental events. *Genes Dev.* **1**, 398-414.

Byerly, L., Cassada, R. C. and Russell, R. L. (1976). The life cycle of the nematode Caenorhabditis elegans. I. Wild-type growth and reproduction. *Dev. Biol.* **51**, 23-33.

Chang, W., Tilmann, C., Thoemke, K., Markussen, F.-H., Mathies, L. D., Kimble, J. and Zarkower, D. (2004). A forkhead protein controls sexual identity of the C. elegans male somatic gonad. *Development* **131**, 1425-1436.

Conte, D., MacNeil, L. T., Walhout, A. J. M. and Mello, C. C. (2015). RNA Interference in Caenorhabditis elegans. *Curr. Protoc. Mol. Biol.* **109**, 26.3.1-26.330.

Dowen, R. H., Breen, P. C., Tullius, T., Conery, A. L. and Ruvkun, G. (2016). A microRNA program in the C. elegans hypodermis couples to intestinal mTORC2/PQM-1 signaling to modulate fat transport. *Genes Dev.* **30**, 1515-1528.

Euling, S. and Ambros, V. R. (1995). Reversal of cell fate determination in Caenorhabditis elegans vulval development. *Development* **122**, 2507-2515.

Euling, S. and Ambros, V. (1996). Heterochronic genes control cell cycle progress and developmental competence of C. elegans vulva precursor cells. *Cell* **84**, 667-676.

Frøkjær-Jensen, C., Davis, M. W., Ailion, M. and Jorgensen, E. M. (2012). Improved Mos1-mediated transgenesis in C. elegans. *Nat. Methods* **9**, 117-118.

Ghosh, S. and Sternberg, P. W. (2014). Spatial and molecular cues for cell outgrowth during C. elegans uterine development. *Dev. Biol.* **396**, 121-135.

Gilleard, J. S., Barry, J. D. and Johnstone, I. L. (1997). cis regulatory requirements for hypodermal cell-specific expression of the Caenorhabditis elegans cuticle collagen gene dpy-7. *Mol. Cell. Biol.* **17**, 2301-2311.

Gissendanner, C. R., Kelley, K., Nguyen, T. Q., Hoener, M. C., Sluder, A. E. and Maina, C. V. (2008). The Caenorhabditis elegans NR4A nuclear receptor is required for spermatheca morphogenesis. *Dev. Biol.* **313**, 767-786.

Hoskins, R., Hajnal, A. F., Harp, S. A. and Kim, S. K. (1996). The C. elegans vulval induction gene lin-2 encodes a member of the MAGUK family of cell junction proteins. *Development* **122**, 97-111.

Iwasaki, K., McCarter, J., Francis, R. and Schedl, T. (1996). emo-1, a Caenorhabditis elegans Sec61p gamma homologue, is required for oocyte development and ovulation. *J. Cell Biol.* **134**, 699-714.

Johnston, W. L., Krizus, A. and Dennis, J. W. (2006). The eggshell is required for meiotic fidelity, polar-body extrusion and polarization of the C. elegans embryo. *BMC Biol.* **4**, 35.

Johnston, W. L., Krizus, A. and Dennis, J. W. (2010). Eggshell chitin and chitin-interacting proteins prevent polyspermy in C. elegans. *Curr. Biol.* **20**, 1932-1937.

Kamath, R. S. and Ahringer, J. (2003). Genome-wide RNAi screening in Caenorhabditis elegans. *Methods* **30**, 313-321.

Kariya, K.-I., Bui, Y. K., Gao, X., Sternberg, P. W. and Kataoka, T. (2004). Phospholipase Cepsilon regulates ovulation in Caenorhabditis elegans. *Dev. Biol.* **274**, 201-210.

Keyte, A. L. and Smith, K. K. (2011). Heterochrony and developmental timing mechanisms: Changing ontogenies in evolution. *Semin. Cell Dev. Biol.* **34**, 99-107.

Kimble, J. and Hirsh, D. (1979). The postembryonic cell lineages of the hermaphrodite and male gonads in Caenorhabditis elegans. *Dev. Biol.* **70**, 396-417.

Klingenberg, C. P. (1998). Heterochrony and allometry: the analysis of evolutionary change in ontogeny. *Biol. Rev. Camb. Philos. Soc.* **73**, 79-123.

Kovacevic, I. and Cram, E. J. (2010). FLN-1/filamin is required for maintenance of actin and exit of fertilized oocytes from the spermatheca in C. elegans. *Dev. Biol.* **347**, 247-257.

Large, E. E. and Mathies, L. D. (2010). hunchback and Ikaros-like zinc finger genes control reproductive system development in Caenorhabditis elegans. *Dev. Biol.* **339**, 51-64.

Liu, Z. and Ambros, V. (1991). Alternative temporal control systems for hypodermal cell differentiation in Caenorhabditis elegans. *Nature* **350**, 162-165.

Maruyama, R., Velarde, N. V., Klancer, R., Gordon, S., Kadandale, P., Parry, J. M., Hang, J. S., Rubin, J., Stewart-Michaelis, A., Schweinsberg, P. et al. (2007). EGG-3 regulates cell-surface and cortex rearrangements during egg activation in Caenorhabditis elegans. *Curr. Biol.* **17**, 1555-1560.

McCarter, J., Bartlett, B., Dang, T. and Schedl, T. (1999). On the control of oocyte meiotic maturation and ovulation in Caenorhabditis elegans. *Dev. Biol.* **205**, 111-128.

Moss, E. G., Lee, R. C. and Ambros, V. (1997). The cold shock domain protein LIN-28 controls developmental timing in C. elegans and is regulated by the lin-4 RNA. *Cell* **88**, 637-646.

Newman, A. P. and Sternberg, P. W. (1996). Coordinated morphogenesis of epithelia during development of the Caenorhabditis elegans uterine-vulval connection. *Proc. Natl. Acad. Sci. USA* **93**, 9329-9333.

Newman, A. P., White, J. G. and Sternberg, P. W. (1996). Morphogenesis of the C. elegans hermaphrodite uterus. *Development* **122**, 3617-3626.

Newman, A. P., Inoue, T., Wang, M. and Sternberg, P. W. (2000). The Caenorhabditis elegans heterochronic gene lin-29 coordinates the vulval–uterine–epidermal connections. *Curr. Biol.* **10**, 1479-1488.

Palmer, R. E., Inoue, T., Sherwood, D. R., Jiang, L. I. and Sternberg, P. W. (2002). Caenorhabditis elegans cog-1 locus Encodes GTX/Nkx6.1 homeodomain proteins and regulates multiple aspects of reproductive system development. *Dev. Biol.* **252**, 202-213.

Pedersen, M. E., Snieckute, G., Kagias, K., Nehammer, C., Multhaupt, H. A. B., Couchman, J. R. and Pocock, R. (2013). An epidermal microRNA regulates neuronal migration through control of the cellular glycosylation state. *Science* **341**, 1404-1408.

Piskounova, E., Polytarchou, C., Thornton, J. E., LaPierre, R. J., Pothoulakis, C., Hagan, J. P., Iliopoulos, D. and Gregory, R. I. (2011). Lin28A and Lin28B inhibit let-7 microRNA biogenesis by distinct mechanisms. *Cell* **147**, 1066-1079.

Reinhart, B. J., Slack, F. J., Basson, M., Pasquinelli, A. E., Bettinger, J. C., Rougvie, a E., Horvitz, H. R. and Ruvkun, G. (2000). The 21-nucleotide let-7 RNA regulates developmental timing in Caenorhabditis elegans. *Nature* **403**, 901-906.

Resnick, T. D., McCulloch, K. A. and Rougvie, A. E. (2010). miRNAs give worms the time of their lives: small RNAs and temporal control in Caenorhabditis elegans. *Dev. Dyn.* **239**, 1477-1489.

Salzberg, Y., Díaz-Balzac, C. A., Ramirez-Suarez, N. J., Attreed, M., Tecle, E., Desbois, M., Kaprielian, Z. and Bülow, H. E. (2013). Skin-derived cues control arborization of sensory dendrites in caenorhabditis elegans. *Cell* **155**, 308-320.

Seggerson, K., Tang, L. and Moss, E. G. (2002). Two genetic circuits repress the Caenorhabditis elegans heterochronic gene lin-28 after translation initiation. *Dev. Biol.* **243**, 215-225.

Shaham, S. (2005). *Methods in Cell Biology*. WormBook.

Shinoda, G., de Soysa, T. Y., Seligson, M. T., Yabuuchi, A., Fujiwara, Y., Yi Huang, P., Hagan, J. P., Gregory, R. I., Moss, E. G. and Daley, G. Q. (2013). Lin28a regulates germ cell pool size and fertility. *Stem Cells* **31**, 1001-1009.

Shirayama, M., Seth, M., Lee, H.-C., Gu, W., Ishidate, T., Conte, D. and Mello, C. C. (2012). piRNAs initiate an epigenetic memory of nonself RNA in the C. elegans germline. *Cell* **150**, 65-77.

Slack, F. J., Basson, M., Liu, Z., Ambros, V., Horvitz, H. R. and Ruvkun, G. (2000). The lin-41 RBCC gene acts in the C. elegans heterochronic pathway between the let-7 regulatory RNA and the LIN-29 transcription factor. *Mol. Cell* **5**, 659-669.

Stiernagle, T. (2006). Maintenance of C. elegans (February 11, 2006), WormBook, ed. The C. elegans Research Community, WormBook.

Stratoulias, V., Heino, T. I. and Michon, F. (2014). Lin-28 regulates oogenesis and muscle formation in Drosophila melanogaster. *PLoS ONE* **9**, e101141.

Vadla, B., Kemper, K., Alaimo, J., Heine, C. and Moss, E. G. (2012). lin-28 controls the succession of cell fate choices via two distinct activities. *PLoS Genet.* **8**, e1002588.

Van Wynsberghe, P. M., Kai, Z. S., Massirer, K. B., Burton, V. H., Yeo, G. W. and Pasquinelli, A. E. (2011). LIN-28 co-transcriptionally binds primary let-7 to regulate miRNA maturation in C. elegans. *Nat. Struct. Mol. Biol.* **18**, 302-308.

Wang, D., Hou, L., Nakamura, S., Su, M., Li, F., Chen, W., Yan, Y., Green, C. D., Chen, D., Zhang, H. et al. (2017). LIN-28 balances longevity and germline stem cell number in Caenorhabditis elegans through let-7/AKT/DAF-16 axis. *Aging Cell* **16**, 113-124.

Wei, X., Potter, C. J., Luo, L. and Shen, K. (2012). Controlling gene expression with the Q repressible binary expression system in Caenorhabditis elegans. *Nat. Methods* **9**, 391-395.

Yochem, J. and Herman, R. K. (2003). Investigating C. elegans development through mosaic analysis. *Development* **130**, 4761-4768.

Yochem, J., Gu, T. and Han, M. (1998). A new marker for mosaic analysis in Caenorhabditis elegans indicates a fusion between hyp6 and hyp7, two major components of the hypodermis. *Genetics* **149**, 1323-1334.

Yu, J., Vodyanik, M. A., Smuga-Otto, K., Antosiewicz-Bourget, J., Frane, J. L., Tian, S., Nie, J., Jonsdottir, G. A., Ruotti, V., Stewart, R. et al. (2007). Induced pluripotent stem cell lines derived from human somatic cells. *Science* **318**, 1917-1920.

Zhang, Y., Foster, J. M., Nelson, L. S., Ma, D. and Carlow, C. K. S. (2005). The chitin synthase genes chs-1 and chs-2 are essential for C. elegans development and responsible for chitin deposition in the eggshell and pharynx, respectively. *Dev. Biol.* **285**, 330-339.

Zhang, J., Ratanasirintrawoot, S., Chandrasekaran, S., Wu, Z., Ficarro, S. B., Yu, C., Ross, C. A., Cacchiarelli, D., Xia, Q., Seligson, M. et al. (2016). LIN28 regulates stem cell metabolism and conversion to primed pluripotency. *Cell Stem Cell* **19**, 66-80.

Zhu, H., Shah, S., Shyh-Chang, N., Shinoda, G., Einhorn, W. S., Viswanathan, S. R., Takeuchi, A., Grasemann, C., Rinn, J. L., Lopez, M. F. et al. (2010). Lin28a transgenic mice manifest size and puberty phenotypes identified in human genetic association studies. *Nat. Genet.* **42**, 626-630.

Zhu, H., Shyh-Chang, N., Segrè, A. V., Shinoda, G., Shah, S. P., Einhorn, W. S., Takeuchi, A., Engreitz, J. M., Hagan, J. P., Kharas, M. G. et al. (2011). The Lin28/let-7 axis regulates glucose metabolism. *Cell* **147**, 81-94.